World Journal of Gastroenterology

Submit a Manuscript: http://www.wjgnet.com/esps/
Help Desk: http://www.wjgnet.com/esps/helpdesk.aspx
DOI: 10.3748/wjg.v22.i20.4835

World J Gastroenterol 2016 May 28; 22(20): 4835-4847
ISSN 1007-9327 (print) ISSN 2219-2840 (online)

REVIEW

Advanced imaging techniques in the therapeutic response of transarterial chemoembolization for hepatocellular carcinoma

Ke Yang, Xiao-Ming Zhang, Lin Yang, Hao Xu, Juan Peng

Ke Yang, Xiao-Ming Zhang, Lin Yang, Hao Xu, Juan Peng, Sichuan Key Laboratory of Medical Imaging, Department of Radiology, Affiliated Hospital of North Sichuan Medical College, Nanchong 637000, Sichuan Province, China

Author contributions: Yang K and Yang L wrote the paper; Zhang XM designed the research; Xu H and Peng J collected the data.

Supported by Projects of Department of Science and Technology of Sichuan Province, No. 2016JY0105.

Conflict-of-interest statement: Authors declare no conflict of interests for this article.

Correspondence to: Lin Yang, MD, Sichuan Key Laboratory of Medical Imaging, Department of Radiology, Affiliated Hospital of North Sichuan Medical College, Wenhua Road No. 63, Nanchong 637000, Sichuan Province, China. linyangmd@163.com
Telephone: +86-817-2262223
Fax: +86-817-2222856

Received: February 26, 2016
Peer-review started: February 28, 2016
First decision: March 21, 2016
Revised: March 29, 2016
Accepted: April 20, 2016
Article in press: April 20, 2016
Published online: May 28, 2016

Abstract

Hepatocellular carcinoma (HCC) is one of the major causes of morbidity and mortality in patients with chronic liver disease. Transarterial chemoembolization (TACE) can significantly improve the survival rate of patients with HCC and is the first treatment choice for patients who are not suitable for surgical resections. The evaluation of the response to TACE treatment affects not only the assessment of the therapy efficacy but also the development of the next step in the treatment plan. The use of imaging to examine changes in tumor volume to assess the response of solid tumors to treatment has been controversial. In recent years, the emergence of new imaging technology has made it possible to observe the response of tumors to treatment prior to any morphological changes. In this article, the advances in studies reporting the use of computed tomography perfusion imaging, diffusion-weighted magnetic resonance imaging (MRI), intravoxel incoherent motion, diffusion kurtosis imaging, magnetic resonance spectroscopy, magnetic resonance perfusion-weighted imaging, blood oxygen level-dependent MRI, positron emission tomography (PET)/computed tomography and PET/MRI to assess the TACE treatment response are reviewed.

Key words: Blood oxygen level-dependent; Computed tomography perfusion imaging; Chemoembolization; Diffusion kurtosis imaging; Diffusion-weighted imaging; Hepatocellular carcinoma; Magnetic resonance perfusion-weighted imaging; Intravoxel incoherent motion; Magnetic resonance spectroscopy

Core tip: Imaging studies play an important role in the evaluation of the response to transarterial chemoembolization treatment. The use of imaging to examine changes in tumor size to assess the response of solid tumors to treatment has been controversial. In recent years, the emergence of new imaging technologies has made it possible to observe the response of tumors to treatment prior to any morphological changes. In this article, we present a summary of the most recent information on the role of imaging in assessing the treatment response in hepatocellular carcinomas.

Yang K, Zhang XM, Yang L, Xu H, Peng J. Advanced imaging techniques in the therapeutic response of transarterial chemoembolization for hepatocellular carcinoma. *World J Gastroenterol* 2016; 22(20): 4835-4847 Available from: URL: http://www.wjgnet.com/1007-9327/full/v22/i20/4835.htm DOI: http://dx.doi.org/10.3748/wjg.v22.i20.4835

INTRODUCTION

Hepatocellular carcinoma (HCC) is one of the major causes of morbidity and mortality in patients with chronic liver disease. Due to the undetected onset of liver cancer, the majority of patients receiving treatment are already in the advanced stage and are no longer candidates for surgical resection. Transarterial chemoembolization (TACE) involves the local infusion of a mixture of chemotherapeutic agents, blocks the blood supply to cancerous lesions and induces ischemia and necrosis in the tumor tissue, thereby significantly improving the survival rate of patients with liver cancer[1-4]. Currently, TACE has been recommended as the standard treatment for patients with stage B (Barcelona Clinic Liver Cancer staging) HCC[5,6]. The assessment of the response of HCC to TACE treatment affects not only the evaluation of the therapeutic efficacy but also the development of the next step in the treatment plan, including the time and frequency of repeated chemoembolization[7]. The previous World Health Organization and Response Evaluation Criteria in Solid Tumors criteria for evaluating the response of solid tumors to treatment depended on the measurement of tumor size[8]. The use of conventional imaging techniques to examine changes in tumor size to assess the response of solid tumors to treatment has been controversial, as many HCC treatments act by inducing tumor necrosis or by reducing vascularity, which is not necessarily accompanied by tumor shrinkage even when response occurs; notably, some tumors clearly respond to treatment but show no remarkable changes in size[9,10]. In recent years, the assessment of tumor viability has attracted increasing attention. The modified Response Evaluation Criteria in Solid Tumors criteria recommended by the European Association for the Study of the Liver consider the treatment factors leading to tumor necrosis and define the lesions that uptake a contrasting agent in the arterial phase as the surviving tumor after treatment[11]. In recent years, the emergence of new imaging technologies has made it possible to observe the response of tumors to treatment prior to any morphological changes. In this article, studies reporting advances in the use of computed tomography perfusion imaging (CTPI), diffusion-weighted magnetic resonance imaging (DWI), intravoxel incoherent motion (IVIM), diffusion kurtosis imaging (DKI), magnetic resonance spectroscopy (MRS), magnetic resonance perfusion-weighted imaging (MR PWI), blood oxygen level-dependent magnetic resonance imaging (BOLD MRI), positron emission tomography/computed tomography (PET/CT) and PET/MRI to assess the response to TACE treatment are reviewed.

COMPUTED TOMOGRAPHY PERFUSION IMAGING

Lipiodol is an ideal embolic agent commonly used in TACE treatment for HCC, and studies have shown that the deposition of lipiodol in the lesions is correlated with antitumor effects[12]. Conventional CT scanning has been widely used in the evaluation and follow-up of the efficacy of TACE treatment for HCC. Though CT can be used to visualize the distribution of lipiodol within the lesions, the high density deposition of lipiodol in tumor tissue can significantly affect the judgment of the viability of the tumor by CT.

CTPI not only clearly shows anatomy of the liver but also reflects changes in liver hemodynamics by allowing the quantitative analysis of blood perfusion in the liver tissue. CTPI performs continuous dynamic scans on selected slices while a contrast agent is intravenously injected, resulting in a curve that reflects the density changes of each pixel within the slice over time (time-density curve). A variety of mathematical models are then used to calculate the various perfusion parameters of the tissues and organs to evaluate the blood perfusion status[13-16] (Figure 1). The main parameters measured by CTPI include hepatic arterial perfusion (HAP), hepatic portal perfusion (HPP), total liver perfusion (TLP), hepatic arterial perfusion index (HAPI), hepatic portal perfusion index (HPPI), blood volume (BV) and mean transit time (MTT). Early CTPI scans used a single-slice continuous dynamic scan mode, but with progress in the development of multi-slice CT and software technology, CTPI has advanced from single-slice perfusion scans to multi-slice and same slice dynamic CT perfusion scans. Currently, spiral CT involving 64 or more slices can be used to conduct full-size liver perfusion scans with greatly improved temporal and spatial resolutions, which allows for the acquisition of more comprehensive hemodynamic information in a single scan. Moreover,

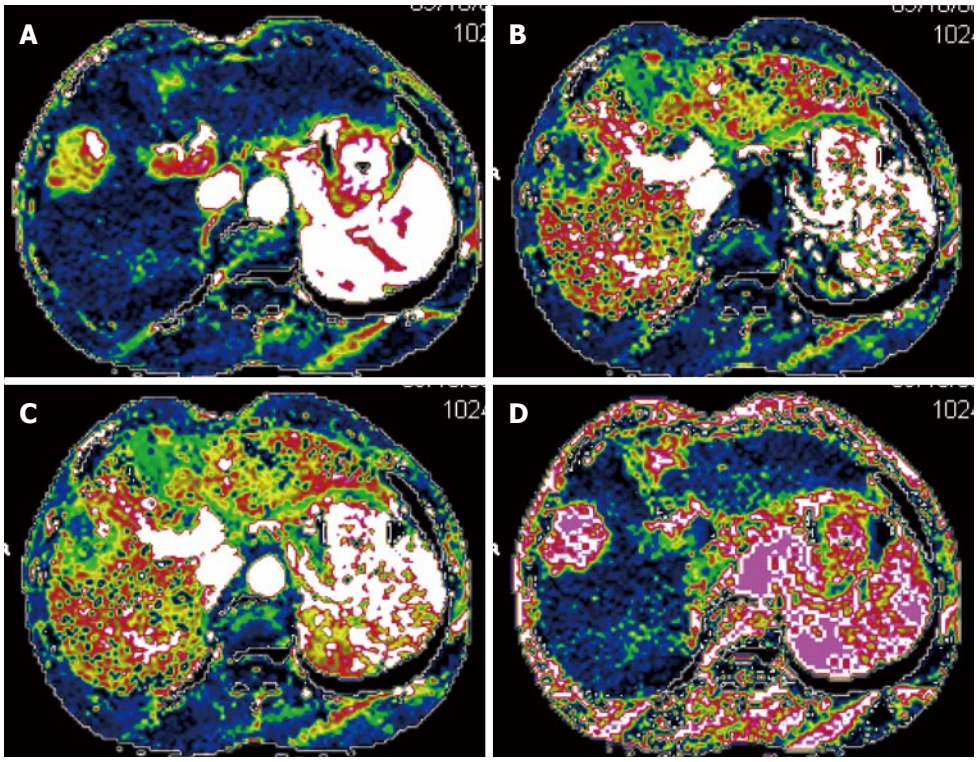

Figure 1 Seventy-year-old male patient with hepatocellular carcinoma. Axial perfusion images of the tumor before transarterial chemoembolization were created by maximum slope method. The tumor showed an increased hepatic arterial perfusion and decreased hepatic portal perfusion compared with the normal parenchyma. The values of hepatic arterial perfusion, hepatic portal perfusion, total liver perfusion and hepatic arterial perfusion index were 0.512 mL/min.mL, 0.226 mL/min.mL, 0.738 mL/min.mL and 69.4%, respectively. A: Image of hepatic arterial perfusion; B: Image of hepatic portal perfusion; C: Image of total liver perfusion; D: Image of hepatic arterial perfusion index.

lesions distant from the hilum can also be measured using CTPI, which has further promoted the clinical application of this technique[17-19].

The blood supply to HCC is one of the main factors affecting the efficacy of TACE treatment[20]. Increased blood supply to the HCC is associated with greater lipiodol accumulation after TACE treatment, whereas reduced blood supply to the HCC results in rather small amounts of lipiodol deposition in the treated lesions[21].

Many investigators have examined the effectiveness of CTPI in evaluating the response of HCC to TACE treatment, suggesting that CT perfusion imaging can accurately measure blood perfusion to the tumor and thus could be used to evaluate the response to TACE therapy[22-27]. Chen *et al*[22] assessed the changes in the CT perfusion parameters pre- and post-TACE in thirty-nine HCC patients in different treatment response groups. In the partial response (PR) treatment response group, the HAP, hepatic arterial fracture (HAF) and hepatic blood volume (HBV) of viable tumors post-TACE were reduced compared with their pre-TACE values. In the stable disease (SD) group, however, none of the CT perfusion parameters were significantly different pre- and post-TACE. In the progressive disease (PD) group, the post-TACE values for HAP, HAF, portal vein perfusion (PVP) and hepatic blood flow (HBF) of viable tumors were significantly increased compared to the pre-TACE values. These results indicated that changes in the CT perfusion parameters of viable tumors are correlated with responses of HCC to TACE, which can be feasibly monitored using CTPI. Reiner *et al*[23] studied sixteen patients with HCC who received CT liver perfusion during the treatment planning stage prior to transarterial radioembolization with Yttrium-90 (90Y) microspheres. The results showed that when responders were compared to non-responders, the 50th and 75th percentiles of arterial perfusion were significantly different and that the response to therapy could be predicted with a sensitivity of 88% and specificity of 75%. Our own studies[9,21] have shown that the CT perfusion parameters of HCC (HAP, TLP and HAPI) significantly decreased after TACE treatment[9] and that the blood perfusion parameters of the HCC lesions were correlated with post-TACE lipiodol deposition. Moreover, increased amounts of blood perfusion were associated with the increased deposition of lipiodol, and vice versa[21]. On the CT perfusion images, the areas with densely deposited lipiodol in the residual lesions in cases with complete or partial response (PR) displayed the complete absence of blood perfusion[9].

These results show that CTPI can be used to accurately measure the changes in perfusion parameters after TACE treatment for HCC and to evaluate the response to TACE therapy prior to changes in tumor size. CTPI can also be used to predict the efficacy of TACE therapy for HCC, to help select appropriate patients for TACE therapy and to develop individualized

treatment programs.

C-arm CT has emerged in recent years and can quantitatively measure the blood volume (BV) changes in tumor tissues. This technique has dramatically increased the convenience of assessing the response to TACE therapy[28-30]. Peynircioğlu *et al*[30] performed radioembolization (n = 21) or TACE (n = 13) treatment on thirty-four patients with HCC and used C-arm CT to measure the tumor BV before and after treatment. These cases were compared to ten cases in which perfusion imaging was performed using multidetector computed tomography (MDCT). The results showed that the mean BV of fourteen tumor lesions in the ten MDCT perfusion patients was highly correlated with the BV values obtained with C-arm CT. After treatment with TACE or radioembolization, the BV values decreased significantly, suggesting that the quantitative BV measurements obtained using C-arm CT are well-correlated with those obtained using MDCT; thus, C-arm CT is a promising tool for monitoring perfusion changes during hepatic arterial embolization. Currently, C-arm CT is mainly used to measure BV, but with the further development of this method, additional parameters can be used in the evaluation of TACE in the clinical treatment of HCC.

The main shortcoming of CTPI is that perfusion CT studies increase radiation exposure. In the future, with improvements to the equipment and technology, the radiation dose will be reduced.

DIFFUSION-WEIGHTED MRI

DWI is currently the only non-invasive imaging technique that can detect the free diffusion motion (Brownian motion) of water molecules in living tissue. Detecting the free diffusion motion of water molecules in the human body enables magnetic resonance at the molecular level. DWI not only reflects the dispersion characteristics of various tissues but also enables quantitative analyses of the microscopic structures and functional changes of tissues and organs. Though DWI has mainly been used in studies of central nervous system diseases[31-33], this technique is increasingly being applied to abdominal examinations[34-42]. At present, the commonly used single-time spin echo-echo planar imaging (SE-EPI) can image in rapid sequence and only takes 20-30 s to complete a liver scan[43], prompting the application of SE-EPI in the diagnosis and treatment of liver diseases.

DWI enables quantitative analyses by measuring the apparent diffusion coefficient (ADC) value. Thus, this technique can be used in assessing the effectiveness of TACE treatment for HCC[44-47]. After TACE therapy for HCC, the tumor cells undergo necrosis and decrease in number, the gaps between cells enlarge, and structures such as the cell membranes are damaged or dissolved, leading to enhanced water diffusion capacity and an increased ADC value. When the tumor survives or recurs, however, the ADC value does not increase or decrease. Bonekamp[44] used TACE therapy to treat seventy-one HCC lesions in forty-eight patients and performed MRI scans before the TACE treatment and one and six months after the treatment to monitor the ADC and venous enhancement (VE) as the tumor changed in size. The results demonstrated that thirty HCC lesions showed PR, thirty-five showed SD, and six showed PD 6 mo after TACE. Increase in ADC and decrease in VE 1 mo after TACE were significantly different between PR, SD, and PD. Yu *et al*[45] used enhanced MRI and DWI scans in twenty-three patients with liver cancer who had received TACE treatment, finding a total of twenty-three recurrent nodules in sixteen cases; the overall sensitivity in DWI was increased from 85.0% to 92.0%, though the specificity was decreased from 65.0% to 50.0%. The pre-TACE tumor ADC can be used to predict the response of HCC to TACE treatment. Mannelli *et al*[47] conducted DWI scans on thirty-six patients receiving TACE treatment for HCC and found that HCCs with poor and incomplete responses to TACE had significantly lower pre-treatment values of ADC and lower post-TACE values of ADC compared to HCCs with good or complete responses.

The shortcomings of DWI include EPI-related artifacts, such as deformation artifacts. Moreover, the ADC values of benign and malignant nodules in the liver overlap to some extent, and discriminating between these values requires a combination of medical history and other test results. Many factors that influence the ADC value, including the MR device, scan parameters (TR and TE), the b-value and the ROI, should be investigated in the future.

INTRAVOXEL INCOHERENT MOTION MR IMAGING

During DWI imaging, the b-value (a gradient factor) determines the sensitivity of the diffusion motion of water molecules in the tissue under analysis while affecting the accuracy of the ADC value. A low b-value enables the acquisition of images with a high SNR but lowers the sensitivity to the diffusion motion, resulting in a higher impact exerted by the blood perfusion on the DWI imaging. Under a high b-value, blood perfusion only has a small impact on DWI imaging, but the tissue contrast is decreased, leading to poor image quality[35,48-50].

IVIM, a multi-b-value diffusion-weighted imaging approach based on the principle of DWI, uses quantitative indicators to show the molecular diffusion and microperfusion of the local capillary network in lesions. The commonly used parameters include the true molecular-diffusion coefficient (D), the perfusion-related diffusion coefficient (D*) and the perfusion fraction (f). Compared with DWI, IVIM better reveals the diffusion effect of water molecules within a lesion

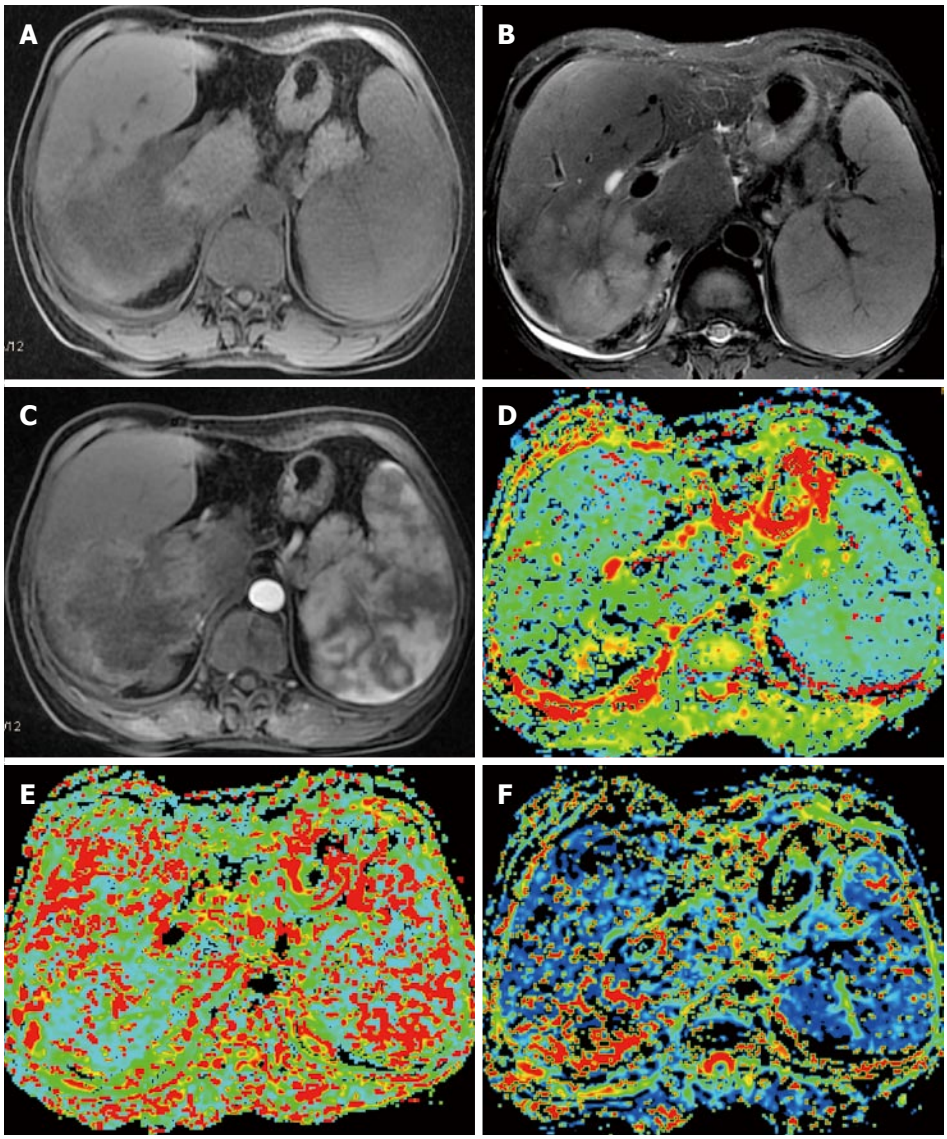

Figure 2 Fifty-three-year-old female patient with hepatocellular carcinoma in the right lobe of the liver. A: Axial T1-weighted image shows a hypointense mass lesion; B: Axial T2-weighted image shows a hyperintense mass lesion; C: Contrast-enhanced MRI during the arterial phase showing lesion enhancement; D: Mapping of the estimated value of the *D* parameter. The average value in the lesion ROI was $D = 1.22 \times 10^{-3}$ mm^2/s; E: Mapping of the estimated value of the *D** parameter. The average value in the lesion ROI was $D^* = 20.6 \times 10^{-3}$ mm^2/s; F: Mapping of the perfusion fraction (f) with a value of 19.6%.

and is thus more conducive to making judgments regarding the nature of liver lesions[51-55]. Watanabe *et al*[51] performed IVIM imaging on a total of 120 liver lesions (including 34 metastases, 32 HCC, 33 hemangiomas and 21 liver cysts) in seventy-four patients and showed that the mean D and ADC values of the benign lesions were greater than those of malignant lesions. The area under the ROC curve for the ADC values was significantly greater than that for the D values, which enabled the differentiation between benign and malignant lesions. When an ADC cut-off value of 1.40 was applied, the sensitivity and specificity for the detection of malignant lesions were 89% and 98%, respectively. Other studies have shown similar results[52-55] (Figure 2).

The applications of IVIM in cancer treatment evaluation have mainly focused on radiotherapy or chemotherapy in head and neck cancers and in breast cancer[56-67]. In recent years, some investigators have applied IVIM in the anti-angiogenesis therapy of liver cancer (including metastatic liver cancer) or radiofrequency ablation therapy[68-73]. Guo *et al*[71] investigated the use of IVIM-DWI to monitor the responses of VX2 tumors to radiofrequency ablation (RF Ablation) therapy in 10 VX2 tumor-bearing rabbits, showing that the IVIM-DWI derived f, D and D* parameters have the potential to indicate the response to therapy immediately after the RF ablation treatment. Shirota *et al*[72] evaluated the association between the therapeutic outcomes of sorafenib for advanced HCC and the parameters of IVIM. Though the true diffusion coefficient (DC) of responders at baseline was significantly higher than that of the non-responders, no significant differences were found in the

other parameters between these two groups. These results indicated that the DC before treatment may be a useful parameter for predicting the therapeutic outcome of using sorafenib to treat advanced HCC.

The use of IVIM to assess the response to TACE treatment in liver cancer has rarely been reported. Park *et al*[74] performed IVIM-DWI and Gd-EOB-DTPA-enhanced MRI scans before TACE therapy in forty-four cases of HCC and conducted CT scans after the TACE treatment. The patients were divided into two groups, the lipiodol good uptake (LGU) group and the lipiodol poor uptake (LPU) group, based on lipiodol deposition, and the results showed that both the arterial enhancement ratio derived from the contrast enhanced MRI and the D* values derived from IVIM-DWI were significantly higher in the LGU group than in the LPU group, indicating that the parameters of IVIM could help to predict lipiodol uptake.

DIFFUSION KURTOSIS IMAGING

The theoretical basis of the DWI and IVIM technologies is that the diffusion of water molecules *in vivo* assumes a normal distribution. In fact, due to the differences in structures and functions of local tissues and cells, the diffusion of water molecules *in vivo* is often a non-normal distribution. DKI is based on the non-normal distribution diffusion of water molecules *in vivo*, and the parameters of DKI measurements include the S, K and D values. DKI is still largely in the research phase, but this technique is being explored in wider clinical studies primarily focused on central nervous system diseases[75-83]. It is encouraging that some investigators have recently begun to use DKI in experiments to investigate its applications in liver diseases both *in vitro* and *in vivo*. Rosenkrantz *et al*[84] performed DKI and DWI scans on *in vitro* samples from twelve HCC cases and showed that the DKI model may provide additional value in characterizing HCC compared to a standard monoexponential model of DWI. Filli *et al*[85] also found that whole-body DKI is technically feasible and may reflect the tissue microstructure more meaningfully than whole-body DWI. Goshima *et al*[86] studied sixty-two consecutive patients with HCC to compare the use of DKI and conventional DWI in assessing the response to treatment. They found that compared to the non-viable group, the mean kurtosis (MK) value and mean ADC value in the viable group were significantly higher and lower, respectively. The sensitivity, specificity and AUC of the ROC curve for the assessment of HCC viability were greater using MK compared to ADC. These results indicated that DKI can be a new option for assessing the post-therapeutic response in HCC.

The results described above indicate that in the near future, DKI will play an important role in evaluating the response of liver cancer to TACE treatment.

MAGNETIC RESONANCE SPECTROSCOPY

Based on chemical shift effects and MRI principles, MRS uses a Fourier transform to process free induction decay signals to convert them into spectra with distributed frequencies. The areas under different metabolic peaks along the MRS frequency axis reflect the different concentrations of different compounds and can be quantitatively measured and analyzed. Thus, MRS not only truly reflects the molecular and chemical compositions of a tissue but also indirectly depicts the metabolism in the tissue[87].

The commonly used nuclei in MRS measurements of the liver are mainly ^{31}P and ^{1}H. By using ^{1}H-MRS to determine the amounts and ratios of choline and its derivatives after TACE treatment for liver cancer, it is possible to know whether HCC survives or relapses after TACE therapy. Studies have shown significant decreases in the choline/lipid values and the absolute value of choline complexes after TACE treatment for liver cancer. Kuo *et al*[88] investigated the use of proton MRS to assess hepatic lesions *in vivo* and the use of a 3.0-T scanner to measure the changes in metabolites related to HCC after TACE treatment. Their study included forty-three consecutive patients with hepatic tumors. Among the patients with proven HCC, eight lesions were evaluated before TACE and two to five days after TACE. A significant difference was achieved in the mean choline/lipid ratio between the malignant and benign tumors, and the mean choline/lipid ratios were significantly decreased after TACE. Wu *et al*[89] also reached similar conclusions. Taken together, those studies indicated that MRS has the potential for use in the detection of early metabolite changes in HCC after TACE[90-92].

The shortcomings of MRS mainly include its rather low sensitivity and specificity in differentiating between small nodules in the liver.

MAGNETIC RESONANCE PERFUSION-WEIGHTED IMAGING

MR PWI is an MRI technology that can reflect the microvascular distribution and blood perfusion in tissues. In MR PWI, a contrast agent is intravenously injected to increase the magnetic sensitivity of local capillaries and induce local magnetic field changes, leading to reduced signals derived from shortened transverse relaxation time by proton spin dephasing in tissues. The fast scanning imaging sequence generates a series of dynamic images; based on these images, the changes in signal intensity of the contrast agent when passing the hepatic parenchyma over time are used to generate the time-intensity curve (TIC), and semi-quantitative parameters such as maximal enhancement (MaxEn), initial enhancement rate (ER)

and initial area under the curve are calculated to indirectly reflect the vascularity and perfusion in the tumor[93]. Quantitative indicators calculated using the Tofts model include K (trans), k (ep) and v (e)[94,95]. The commonly used PWI sequences include enhanced spin labeling MRI (arterial spin labeling, ASL), T2*-weighted contrast-enhanced dynamic magnetic susceptibility MRI (dynamic susceptibility contrast, DSC) and T1-weighted dynamic contrast-enhanced MRI (dynamic contrast enhancement, DCE). ASL-MRI and DSC-MRI have been mostly used in PWI studies of the brain, whereas the DCE-MRI sequence has been frequently used in PWI studies of the liver[93]. PWI is a new technology that can improve the sensitivity and specificity of liver disease diagnoses. With its high temporal and spatial resolutions, PWI can directly reflect the blood perfusion of the subject tissue and indirectly reflect the tissue's microvascular distribution. This technique better displays the lesions and tremendously helps facilitate the analysis of the disease, the identification of benign and malignant lesions and the assessment of the response to TACE treatment[96-102]. Xu *et al*[96] investigated the value of perfusion-weighted MRI in the evaluation of the intranodular hemodynamic characteristics of dysplastic nodules (DNs) and HCCs in an experimental rat model. A total of 40 rats with chemically induced DNs and HCCs were investigated. Time to peak (Tp), maximal relative signal enhancement (REmax) and the initial slope of the signal intensity (SI) *vs* the time curves of the nodules and cirrhotic liver tissues were evaluated. The nodules that precisely corresponded to the MRI were examined histologically, and the results showed that HCCs had a significantly higher REmax, a shorter Tp and a higher slope than the adjacent cirrhotic liver. The REmax and slope of DNs were significantly lower than the adjacent cirrhotic liver parenchyma. Chen *et al*[97] performed MR PWI scans in thirty-five cases of HCC 24-48 h before and 48-168 h after TACE treatment, finding that in thirty-four of the HCC patients, the time-signal intensity curve (TSC) before TACE quickly decreased and then slowly increased in the tumor region of interest. After TACE, the fluctuating range of the TSC was significantly reduced in thirty-one patients, slightly reduced in three and not significantly changed in one. These results show that MR PWI is highly useful in the clinical evaluation of the efficacy of TACE in treating HCC.

Compared with CTPI, MR PWI has a higher temporal resolution, requires a smaller dose of contrast agent and poses no risk of radiation injury. However, this spectroscopic imaging technique requires more specialized equipment, has a longer imaging time and is thus more affected by environmental factors (*e.g.*, respiratory motion and the shifts caused by respiratory motion of the target lesions, *etc.*). Moreover, the heavy load on data processing has limited the clinical application and promotion of PWI.

BLOOD OXYGEN LEVEL DEPENDENT MRI

Ogawa *et al*[103] believed that paramagnetic deoxyhemoglobin could be used as a natural contrast agent in MRI scans and that deoxyhemoglobin might have contrast effects that could be observed using a gradient echo sequence in high-magnetic field. Based on these effects, these authors investigated whether determining the microvascular blood oxygen content could be used to reflect the dynamics and pathophysiology of blood flow in organs and tissues[103,104]. *In vivo*, paramagnetic deoxyhemoglobin forms a small magnetic field and a magnetic field gradient in its surroundings, causing heterogeneity in the magnetic field within the local tissue and shortening the T2*-weighted signal. The blood oxyhemoglobin and deoxyhemoglobin have opposite magnetic properties, and when the blood flow in the local tissue and the relative amount of oxygenated hemoglobin increase, the T2*-shortening effect of deoxygenated hemoglobin weakens, causing elongated local T2*, and vice versa. Because the value of the transverse relaxation rate (R2*) and the deoxyhemoglobin concentration in the tissue are correlated, in practice, the R2* value is used as an indicator for the quantitative evaluation of changes in the oxygen content in the local tissue.

The BOLD MRI technique, which has been successfully applied in studies of the central nervous system and urogenital system[105-112], is still in the exploratory stage for the diagnosis and treatment of liver cancer. Choi *et al*[113] studied the feasibility of using carbogen-challenge BOLD MRI to assess the early response of liver tumors to chemoembolization in a rat hepatoma model. Their results demonstrated that there was a significant difference between the pre-chemoembolization and post-chemoembolization percentages by which the R2* values of the tumors changed. Zhang *et al*[114] evaluated the feasibility of performing carbogen gas-challenge BOLD MRI measurements in patients with HCC and found that in two cases, the R2* values were significantly decreased one day after TACE. These findings indicated the feasibility of using BOLD MRI to evaluate the response of liver cancer to TACE treatment.

The shortcomings of BOLD MRI are that the technology is susceptible to influences of plasma proteins, molecular diffusion, pH, temperature, pixels, blood flow and vascular course. The iron stored in the liver may also affect the results. Plotting the ROI and analyzing the R2* value are susceptible to the influences of factors such as partial volume effects, blood vessels, necrosis, and bleeding. In future research, BOLD MRI technology will play an important role in evaluating the use of TACE to treat liver cancer.

PET/CT AND PET/MRI

PET/CT can reveal the metabolic information of

tumor tissues at the molecular level and can be used to diagnose malignant cancer with high sensitivity and specificity. Fluoro-deoxy-glucose (18F-FDG) is a glucose analogue that can reflect glucose metabolism in the tissue. Because changes in tissue metabolism always precede changes in tissue structure, PET/CT can be used to assess the early response after TACE treatment and to show residual, recurring and metastasized lesions by quantitatively analyzing the changes in the standardized uptake value (SUV) of the HCC lesions before and after TACE treatment[115-120]. Kim *et al*[115] performed PET/CT and enhanced CT scans on thirty-eight liver cancer lesions in thirty-six patients after TACE therapy and found that for the viable residual lesions, the diagnostic sensitivities of PET/CT and contrast-enhanced CT in the early postembolic period were 100% and 94%, respectively; in the late postembolic period, these values were 93% and 79%, respectively. When the multiphasic CT was normal, the 18F-FDG PET/CT could clearly reveal intrahepatic tumor recurrence and/or extrahepatic metastases in patients with elevated AFP after TACE treatment for HCC[119,120].

Due to the high cost of PET/CT examination and the high radiation dose, this method is not suitable for use in the routine evaluation of TACE treatment.

PET/MRI combines the advantages of PET and MRI. This method not only provides a better soft tissue contrast than PET/CT, thus providing richer information on molecular function and form, but also overcomes the body damage caused by CT irradiation during a PET/CT examination and the false positives found in PET/CT images. Although PET/MRI is a very recent technology, preliminary studies have already shown that PET/MRI has a great potential for applications in the nervous system, cardiovascular system and neoplastic diseases[121-125]. Yu *et al*[126] reported that the additional value of functional MRI techniques in combination with PET must be considered; MR DWI, for example, has been demonstrated to significantly improve the detection of sub-centimeter sized intrahepatic HCC metastases compared with conventional liver MRI alone (84% *vs* 69%). Tsouana *et al*[127] employed hybrid 18F-Fluroethyl-Choline (FEC) PET)/MRI to evaluate the treatment response of four cases of intracranial non-germinomatous germ cell tumors, and the results showed that in two patients, faint or absent choline avidity correlated with negative histology, whereas in two other patients, persistent choline avidity in the residual mass suggested the presence of a viable tumor, which was subsequently confirmed histologically.

Currently, the use of PET/MRI to evaluate interventional treatment for HCC has been rarely reported. Fowler *et al*[128] studied the relationship between dose deposition measured by PET/MRI and the response of individual lesions to radioembolization with 90Y microspheres. Twenty-six patients undergoing lobar treatment with 90Y microspheres underwent PET/MRI within 66 h of treatment and had follow-up imaging available. The results showed that the average dose could be used to predict the responses of responders and non-responders for all lesion types. PET/MRI of the 90Y microsphere distribution in patients with colorectal metastases showed significantly higher dose volume histograms (DVHs) values for responders than non-responders. A DVH analysis of the 90Y microsphere distribution following treatment may be an important predictor of response and could be used to guide future adaptive therapy trials. With the development of PET/MRI, this technology will provide more useful information for the evaluation of interventional liver cancer treatments.

CONCLUSION

In recent years, emerging imaging techniques such as new functional imaging have been effectively used to evaluate the early response of HCC to TACE treatment. Because different imaging techniques have their own advantages and disadvantages, to detect cancer lesions as early as possible and to provide accurate information regarding the diagnosis, staging and treatment evaluation, clinical applications should combine multiple imaging techniques according to the specific circumstances such that the advantages of each technique can compensate for the shortcomings of other techniques, thereby providing a comprehensive evaluation of the lesion[129,130]. With the rapid development of medical imaging, imaging technology will play an increasingly important role in cancer diagnosis and the evaluation of the treatment response.

REFERENCES

1 **Lo CM**, Ngan H, Tso WK, Liu CL, Lam CM, Poon RT, Fan ST, Wong J. Randomized controlled trial of transarterial lipiodol chemoembolization for unresectable hepatocellular carcinoma. *Hepatology* 2002; **35**: 1164-1171 [PMID: 11981766 DOI: 10.1053/jhep.2002.33156]

2 **Song do S**, Nam SW, Bae SH, Kim JD, Jang JW, Song MJ, Lee SW, Kim HY, Lee YJ, Chun HJ, You YK, Choi JY, Yoon SK. Outcome of transarterial chemoembolization-based multi-modal treatment in patients with unresectable hepatocellular carcinoma. *World J Gastroenterol* 2015; **21**: 2395-2404 [PMID: 25741147 DOI: 10.3748/wjg.v21.i8.2395]

3 **Marelli L**, Stigliano R, Triantos C, Senzolo M, Cholongitas E, Davies N, Tibballs J, Meyer T, Patch DW, Burroughs AK. Transarterial therapy for hepatocellular carcinoma: which technique is more effective? A systematic review of cohort and randomized studies. *Cardiovasc Intervent Radiol* 2007; **30**: 6-25 [PMID: 17103105 DOI: 10.1007/s00270-006-0062-3]

4 **Llovet JM**, Real MI, Montaña X, Planas R, Coll S, Aponte J, Ayuso C, Sala M, Muchart J, Solà R, Rodés J, Bruix J. Arterial embolisation or chemoembolisation versus symptomatic treatment in patients with unresectable hepatocellular carcinoma: a randomised controlled trial. *Lancet* 2002; **359**: 1734-1739 [PMID: 12049862 DOI: 10.1016/s0140-6736(02)08649-x]

5 **European Association For The Study Of The Liver, European Organisation For Research And Treatment Of Cancer**. EASL-EORTC clinical practice guidelines: management of hepatocellular carcinoma. *J Hepatol* 2012; **56**: 908-943 [PMID: 22424438 DOI:

10.1016/j.jhep.2011.12.001]
6 **Bruix J**, Sherman M. Management of hepatocellular carcinoma: an update. *Hepatology* 2011; **53**: 1020-1022 [PMID: 21374666 DOI: 10.1002/hep.24199]
7 **Lim HK**, Han JK. Hepatocellular carcinoma: evaluation of therapeutic response to interventional procedures. *Abdom Imaging* 2002; **27**: 168-179 [PMID: 11847576 DOI: 10.1007/s00261-001-0093-9]
8 **Therasse P**, Arbuck SG, Eisenhauer EA, Wanders J, Kaplan RS, Rubinstein L, Verweij J, Van Glabbeke M, van Oosterom AT, Christian MC, Gwyther SG. New guidelines to evaluate the response to treatment in solid tumors. European Organization for Research and Treatment of Cancer, National Cancer Institute of the United States, National Cancer Institute of Canada. *J Natl Cancer Inst* 2000; **92**: 205-216 [PMID: 10655437 DOI: 10.1093/jnci/92.3.205]
9 **Yang L**, Zhang XM, Tan BX, Liu M, Dong GL, Zhai ZH. Computed tomographic perfusion imaging for the therapeutic response of chemoembolization for hepatocellular carcinoma. *J Comput Assist Tomogr* 2012; **36**: 226-230 [PMID: 22446364 DOI: 10.1097/RCT.0b013e318245c23c]
10 **Kamel IR**, Liapi E, Reyes DK, Zahurak M, Bluemke DA, Geschwind JF. Unresectable hepatocellular carcinoma: serial early vascular and cellular changes after transarterial chemoembolization as detected with MR imaging. *Radiology* 2009; **250**: 466-473 [PMID: 19188315 DOI: 10.1148/radiol.2502072222]
11 **Arora A**, Kumar A. Treatment Response Evaluation and Follow-up in Hepatocellular Carcinoma. *J Clin Exp Hepatol* 2014; **4**: S126-S129 [PMID: 25755604 DOI: 10.1016/j.jceh.2014.05.005]
12 **Kanematsu T**, Furuta T, Takenaka K, Matsumata T, Yoshida Y, Nishizaki T, Hasuo K, Sugimachi K. A 5-year experience of lipiodolization: selective regional chemotherapy for 200 patients with hepatocellular carcinoma. *Hepatology* 1989; **10**: 98-102 [PMID: 2544499 DOI: 10.1002/hep.1840100119]
13 **Miles KA**, Hayball M, Dixon AK. Colour perfusion imaging: a new application of computed tomography. *Lancet* 1991; **337**: 643-645 [PMID: 1671994 DOI: 10.1016/0140-6736(91)92455-B]
14 **Miles KA**. Measurement of tissue perfusion by dynamic computed tomography. *Br J Radiol* 1991; **64**: 409-412 [PMID: 2036562 DOI: 10.1259/0007-1285-64-761-409]
15 **Miles KA**, Hayball MP, Dixon AK. Functional images of hepatic perfusion obtained with dynamic CT. *Radiology* 1993; **188**: 405-411 [PMID: 8327686 DOI: 10.1148/radiology.188.2.8327686]
16 **Miles KA**, Hayball MP, Dixon AK. Measurement of human pancreatic perfusion using dynamic computed tomography with perfusion imaging. *Br J Radiol* 1995; **68**: 471-475 [PMID: 7788231 DOI: 10.1259/0007-1285-68-809-471]
17 **Singh J**, Sharma S, Aggarwal N, Sood RG, Sood S, Sidhu R. Role of Perfusion CT Differentiating Hemangiomas from Malignant Hepatic Lesions. *J Clin Imaging Sci* 2014; **4**: 10 [PMID: 24744967 DOI: 10.4103/2156-7514.127959]
18 **Thaiss WM**, Haberland U, Kaufmann S, Spira D, Thomas C, Nikolaou K, Horger M, Sauter AW. Iodine concentration as a perfusion surrogate marker in oncology: Further elucidation of the underlying mechanisms using Volume Perfusion CT with 80 kVp. *Eur Radiol* 2015; Epub ahead of print [PMID: 26679179 DOI: 10.1007/s00330-015-4154-9]
19 **Kaufmann S**, Horger T, Oelker A, Kloth C, Nikolaou K, Schulze M, Horger M. Characterization of hepatocellular carcinoma (HCC) lesions using a novel CT-based volume perfusion (VPCT) technique. *Eur J Radiol* 2015; **84**: 1029-1035 [PMID: 25816994 DOI: 10.1016/j.ejrad.2015.02.020]
20 **Vogl TJ**, Schaefer P, Lehnert T, Nour-Eldin NE, Ackermann H, Mbalisike E, Hammerstingl R, Eichler K, Zangos S, Naguib NN. Intraprocedural blood volume measurement using C-arm CT as a predictor for treatment response of malignant liver tumours undergoing repetitive transarterial chemoembolization (TACE). *Eur Radiol* 2016; **26**: 755-763 [PMID: 26123407 DOI: 10.1007/s00330-015-3869-y]
21 **Yang L**, Zhang XM, Zhou XP, Tang W, Guan YS, Zhai ZH, Dong GL. Correlation between tumor perfusion and lipiodol deposition in hepatocellular carcinoma after transarterial chemoembolization. *J Vasc Interv Radiol* 2010; **21**: 1841-1846 [PMID: 20980165 DOI: 10.1016/j.jvir.2010.08.015]
22 **Chen G**, Ma DQ, He W, Zhang BF, Zhao LQ. Computed tomography perfusion in evaluating the therapeutic effect of transarterial chemoembolization for hepatocellular carcinoma. *World J Gastroenterol* 2008; **14**: 5738-5743 [PMID: 18837093 DOI: 10.3748/wjg.14.5738]
23 **Reiner CS**, Gordic S, Puippe G, Morsbach F, Wurnig M, Schaefer N, Veit-Haibach P, Pfammatter T, Alkadhi H. Histogram Analysis of CT Perfusion of Hepatocellular Carcinoma for Predicting Response to Transarterial Radioembolization: Value of Tumor Heterogeneity Assessment. *Cardiovasc Intervent Radiol* 2016; **39**: 400-408 [PMID: 26216725 DOI: 10.1007/s00270-015-1185-1]
24 **Kan Z**, Kobayashi S, Phongkitkarun S, Charnsangavej C. Functional CT quantification of tumor perfusion after transhepatic arterial embolization in a rat model. *Radiology* 2005; **237**: 144-150 [PMID: 16183930 DOI: 10.1148/radiol.2371040526]
25 **Tsushima Y**, Funabasama S, Aoki J, Sanada S, Endo K. Quantitative perfusion map of malignant liver tumors, created from dynamic computed tomography data. *Acad Radiol* 2004; **11**: 215-223 [PMID: 14974597 DOI: 10.1016/S1076-6332(03)00578-6]
26 **Ippolito D**, Fior D, Bonaffini PA, Capraro C, Leni D, Corso R, Sironi S. Quantitative evaluation of CT-perfusion map as indicator of tumor response to transarterial chemoembolization and radiofrequency ablation in HCC patients. *Eur J Radiol* 2014; **83**: 1665-1671 [PMID: 24962900 DOI: 10.1016/j.ejrad.2014.05.040]
27 **Ippolito D**, Bonaffini PA, Ratti L, Antolini L, Corso R, Fazio F, Sironi S. Hepatocellular carcinoma treated with transarterial chemoembolization: dynamic perfusion-CT in the assessment of residual tumor. *World J Gastroenterol* 2010; **16**: 5993-6000 [PMID: 21157976 DOI: 10.3748/wjg.v16.i47.5993]
28 **Syha R**, Grözinger G, Grosse U, Maurer M, Zender L, Horger M, Nikolaou K, Ketelsen D. Parenchymal Blood Volume Assessed by C-Arm-Based Computed Tomography in Immediate Posttreatment Evaluation of Drug-Eluting Bead Transarterial Chemoembolization in Hepatocellular Carcinoma. *Invest Radiol* 2016; **51**: 121-126 [PMID: 26488373 DOI: 10.1097/rli.0000000000000215]
29 **Syha R**, Grözinger G, Grosse U, Maurer M, Zender L, Horger M, Nikolaou K, Ketelsen D. C-arm computed tomography parenchymal blood volume measurement in evaluation of hepatocellular carcinoma before transarterial chemoembolization with drug eluting beads. *Cancer Imaging* 2015; **15**: 22 [PMID: 26715200 DOI: 10.1186/s40644-015-0057-x]
30 **Peynircioğlu B**, Hızal M, Çil B, Deuerling-Zheng Y, Von Roden M, Hazırolan T, Akata D, Özmen M, Balkancı F. Quantitative liver tumor blood volume measurements by a C-arm CT post-processing software before and after hepatic arterial embolization therapy: comparison with MDCT perfusion. *Diagn Interv Radiol* 2015; **21**: 71-77 [PMID: 25538037 DOI: 10.5152/dir.2014.13290]
31 **Mehdizade A**, Somon T, Wetzel S, Kelekis A, Martin JB, Scheidegger JR, Sztajzel R, Lovblad KO, Ruefenacht DA, Delavelle J. Diffusion weighted MR imaging on a low-field open magnet. Comparison with findings at 1.5T in 18 patients with cerebral ischemia. *J Neuroradiol* 2003; **30**: 25-30 [PMID: 12624588]
32 **Igarashi H**. What stroke MRI provides to us. *Rinsho Shinkeigaku* 2007; **47**: 921-924 [PMID: 18210836]
33 **Schellinger PD**, Bryan RN, Caplan LR, Detre JA, Edelman RR, Jaigobin C, Kidwell CS, Mohr JP, Sloan M, Sorensen AG, Warach S. Evidence-based guideline: The role of diffusion and perfusion MRI for the diagnosis of acute ischemic stroke: report of the Therapeutics and Technology Assessment Subcommittee of the American Academy of Neurology. *Neurology* 2010; **75**: 177-185 [PMID: 20625171 DOI: 10.1212/WNL.0b013e3181e7c9dd]
34 **Kele PG**, van der Jagt EJ. Diffusion weighted imaging in the liver. *World J Gastroenterol* 2010; **16**: 1567-1576 [PMID: 20355235 DOI: 10.3748/wjg.v16.i13.1567]
35 **Dijkstra H**, Baron P, Kappert P, Oudkerk M, Sijens PE. Effects of microperfusion in hepatic diffusion weighted imaging. *Eur Radiol* 2012; **22**: 891-899 [PMID: 22080250 DOI: 10.1007/

s00330-011-2313-1]
36 **Chung WS**, Kim MJ, Chung YE, Kim YE, Park MS, Choi JY, Kim KW. Comparison of gadoxetic acid-enhanced dynamic imaging and diffusion-weighted imaging for the preoperative evaluation of colorectal liver metastases. *J Magn Reson Imaging* 2011; **34**: 345-353 [PMID: 21702068 DOI: 10.1002/jmri.22671]
37 **Sandrasegaran K**, Akisik FM, Lin C, Tahir B, Rajan J, Saxena R, Aisen AM. Value of diffusion-weighted MRI for assessing liver fibrosis and cirrhosis. *AJR Am J Roentgenol* 2009; **193**: 1556-1560 [PMID: 19933647 DOI: 10.2214/ajr.09.2436]
38 **Lambregts DM**, Vandecaveye V, Barbaro B, Bakers FC, Lambrecht M, Maas M, Haustermans K, Valentini V, Beets GL, Beets-Tan RG. Diffusion-weighted MRI for selection of complete responders after chemoradiation for locally advanced rectal cancer: a multicenter study. *Ann Surg Oncol* 2011; **18**: 2224-2231 [PMID: 21347783 DOI: 10.1245/s10434-011-1607-5]
39 **Kim SY**, Lee SS, Byun JH, Park SH, Kim JK, Park B, Kim N, Lee MG. Malignant hepatic tumors: short-term reproducibility of apparent diffusion coefficients with breath-hold and respiratory-triggered diffusion-weighted MR imaging. *Radiology* 2010; **255**: 815-823 [PMID: 20501719 DOI: 10.1148/radiol.10091706]
40 **Heo SH**, Jeong YY, Shin SS, Kim JW, Lim HS, Lee JH, Koh YS, Cho CK, Kang HK. Apparent diffusion coefficient value of diffusion-weighted imaging for hepatocellular carcinoma: correlation with the histologic differentiation and the expression of vascular endothelial growth factor. *Korean J Radiol* 2010; **11**: 295-303 [PMID: 20461183 DOI: 10.3348/kjr.2010.11.3.295]
41 **Nasu K**, Kuroki Y, Tsukamoto T, Nakajima H, Mori K, Minami M. Diffusion-weighted imaging of surgically resected hepatocellular carcinoma: imaging characteristics and relationship among signal intensity, apparent diffusion coefficient, and histopathologic grade. *AJR Am J Roentgenol* 2009; **193**: 438-444 [PMID: 19620441 DOI: 10.2214/ajr.08.1424]
42 **Jiang ZX**, Peng WJ, Li WT, Tang F, Liu SY, Qu XD, Wang JH, Lu HF. Effect of b value on monitoring therapeutic response by diffusion-weighted imaging. *World J Gastroenterol* 2008; **14**: 5893-5899 [PMID: 18855990 DOI: 10.3748/wjg.14.5893]
43 **Wybranski C**, Zeile M, Löwenthal D, Fischbach F, Pech M, Röhl FW, Gademann G, Ricke J, Dudeck O. Value of diffusion weighted MR imaging as an early surrogate parameter for evaluation of tumor response to high-dose-rate brachytherapy of colorectal liver metastases. *Radiat Oncol* 2011; **6**: 43 [PMID: 21524305 DOI: 10.1186/1748-717x-6-43]
44 **Bonekamp S**, Jolepalem P, Lazo M, Gulsun MA, Kiraly AP, Kamel IR. Hepatocellular carcinoma: response to TACE assessed with semiautomated volumetric and functional analysis of diffusion-weighted and contrast-enhanced MR imaging data. *Radiology* 2011; **260**: 752-761 [PMID: 21771960 DOI: 10.1148/radiol.11102330]
45 **Yu JS**, Kim JH, Chung JJ, Kim KW. Added value of diffusion-weighted imaging in the MRI assessment of perilesional tumor recurrence after chemoembolization of hepatocellular carcinomas. *J Magn Reson Imaging* 2009; **30**: 153-160 [PMID: 19557734 DOI: 10.1002/jmri.21818]
46 **Kubota K**, Yamanishi T, Itoh S, Murata Y, Miyatake K, Yasunami H, Morio K, Hamada N, Nishioka A, Ogawa Y. Role of diffusion-weighted imaging in evaluating therapeutic efficacy after transcatheter arterial chemoembolization for hepatocellular carcinoma. *Oncol Rep* 2010; **24**: 727-732 [PMID: 20664980 DOI: 10.3892/or_00000914]
47 **Mannelli L**, Kim S, Hajdu CH, Babb JS, Taouli B. Serial diffusion-weighted MRI in patients with hepatocellular carcinoma: Prediction and assessment of response to transarterial chemoembolization. Preliminary experience. *Eur J Radiol* 2013; **82**: 577-582 [PMID: 23246330 DOI: 10.1016/j.ejrad.2012.11.026]
48 **Thoeny HC**, De Keyzer F. Diffusion-weighted MR imaging of native and transplanted kidneys. *Radiology* 2011; **259**: 25-38 [PMID: 21436095 DOI: 10.1148/radiol.10092419]
49 **Agnello F**, Ronot M, Valla DC, Sinkus R, Van Beers BE, Vilgrain V. High-b-value diffusion-weighted MR imaging of benign hepatocellular lesions: quantitative and qualitative analysis. *Radiology* 2012; **262**: 511-519 [PMID: 22143926 DOI: 10.1148/radiol.11110922]
50 **Taouli B**, Tolia AJ, Losada M, Babb JS, Chan ES, Bannan MA, Tobias H. Diffusion-weighted MRI for quantification of liver fibrosis: preliminary experience. *AJR Am J Roentgenol* 2007; **189**: 799-806 [PMID: 17885048 DOI: 10.2214/ajr.07.2086]
51 **Watanabe H**, Kanematsu M, Goshima S, Kajita K, Kawada H, Noda Y, Tatahashi Y, Kawai N, Kondo H, Moriyama N. Characterizing focal hepatic lesions by free-breathing intravoxel incoherent motion MRI at 3.0 T. *Acta Radiol* 2014; **55**: 1166-1173 [PMID: 24316660 DOI: 10.1177/0284185113514966]
52 **Yamada I**, Aung W, Himeno Y, Nakagawa T, Shibuya H. Diffusion coefficients in abdominal organs and hepatic lesions: evaluation with intravoxel incoherent motion echo-planar MR imaging. *Radiology* 1999; **210**: 617-623 [PMID: 10207458 DOI: 10.1148/radiology.210.3.r99fe17617]
53 **Penner AH**, Sprinkart AM, Kukuk GM, Gütgemann I, Gieseke J, Schild HH, Willinek WA, Mürtz P. Intravoxel incoherent motion model-based liver lesion characterisation from three b-value diffusion-weighted MRI. *Eur Radiol* 2013; **23**: 2773-2783 [PMID: 23666233 DOI: 10.1007/s00330-013-2869-z]
54 **Ichikawa S**, Motosugi U, Ichikawa T, Sano K, Morisaka H, Araki T. Intravoxel incoherent motion imaging of focal hepatic lesions. *J Magn Reson Imaging* 2013; **37**: 1371-1376 [PMID: 23172819 DOI: 10.1002/jmri.23930]
55 **Woo S**, Lee JM, Yoon JH, Joo I, Han JK, Choi BI. Intravoxel incoherent motion diffusion-weighted MR imaging of hepatocellular carcinoma: correlation with enhancement degree and histologic grade. *Radiology* 2014; **270**: 758-767 [PMID: 24475811 DOI: 10.1148/radiol.13130444]
56 **Xiao Y**, Pan J, Chen Y, Chen Y, He Z, Zheng X. Intravoxel Incoherent Motion-Magnetic Resonance Imaging as an Early Predictor of Treatment Response to Neoadjuvant Chemotherapy in Locoregionally Advanced Nasopharyngeal Carcinoma. *Medicine* (Baltimore) 2015; **94**: e973 [PMID: 26091468 DOI: 10.1097/md.0000000000000973]
57 **Kim DY**, Kim HS, Goh MJ, Choi CG, Kim SJ. Utility of intravoxel incoherent motion MR imaging for distinguishing recurrent metastatic tumor from treatment effect following gamma knife radiosurgery: initial experience. *AJNR Am J Neuroradiol* 2014; **35**: 2082-2090 [PMID: 24970548 DOI: 10.3174/ajnr.A3995]
58 **Hauser T**, Essig M, Jensen A, Laun FB, Münter M, Maier-Hein KH, Stieltjes B. Prediction of treatment response in head and neck carcinomas using IVIM-DWI: Evaluation of lymph node metastasis. *Eur J Radiol* 2014; **83**: 783-787 [PMID: 24631600 DOI: 10.1016/j.ejrad.2014.02.013]
59 **Hauser T**, Essig M, Jensen A, Gerigk L, Laun FB, Münter M, Simon D, Stieltjes B. Characterization and therapy monitoring of head and neck carcinomas using diffusion-imaging-based intravoxel incoherent motion parameters-preliminary results. *Neuroradiology* 2013; **55**: 527-536 [PMID: 23417120 DOI: 10.1007/s00234-013-1154-9]
60 **Hu YC**, Yan LF, Wu L, Du P, Chen BY, Wang L, Wang SM, Han Y, Tian Q, Yu Y, Xu TY, Wang W, Cui GB. Intravoxel incoherent motion diffusion-weighted MR imaging of gliomas: efficacy in preoperative grading. *Sci Rep* 2014; **4**: 7208 [PMID: 25434593 DOI: 10.1038/srep07208]
61 **Zhang SX**, Jia QJ, Zhang ZP, Liang CH, Chen WB, Qiu QH, Li H. Intravoxel incoherent motion MRI: emerging applications for nasopharyngeal carcinoma at the primary site. *Eur Radiol* 2014; **24**: 1998-2004 [PMID: 24838795 DOI: 10.1007/s00330-014-3203-0]
62 **Marzi S**, Forina C, Marucci L, Giovinazzo G, Giordano C, Piludu F, Landoni V, Spriano G, Vidiri A. Early radiation-induced changes evaluated by intravoxel incoherent motion in the major salivary glands. *J Magn Reson Imaging* 2015; **41**: 974-982 [PMID: 24700435 DOI: 10.1002/jmri.24626]
63 **Kim HS**, Suh CH, Kim N, Choi CG, Kim SJ. Histogram analysis of intravoxel incoherent motion for differentiating recurrent tumor from treatment effect in patients with glioblastoma: initial clinical experience. *AJNR Am J Neuroradiol* 2014; **35**: 490-497 [PMID:

23969343 DOI: 10.3174/ajnr.A3719]
64 **Cui Y**, Zhang C, Li X, Liu H, Yin B, Xu T, Zhang Y, Wang D. Intravoxel Incoherent Motion Diffusion-weighted Magnetic Resonance Imaging for Monitoring the Early Response to ZD6474 from Nasopharyngeal Carcinoma in Nude Mouse. *Sci Rep* 2015; **5**: 16389 [PMID: 26574153 DOI: 10.1038/srep16389]
65 **Ding Y**, Hazle JD, Mohamed AS, Frank SJ, Hobbs BP, Colen RR, Gunn GB, Wang J, Kalpathy-Cramer J, Garden AS, Lai SY, Rosenthal DI, Fuller CD. Intravoxel incoherent motion imaging kinetics during chemoradiotherapy for human papillomavirus-associated squamous cell carcinoma of the oropharynx: preliminary results from a prospective pilot study. *NMR Biomed* 2015; **28**: 1645-1654 [PMID: 26451969 DOI: 10.1002/nbm.3412]
66 **Che S**, Zhao X, Ou Y, Li J, Wang M, Wu B, Zhou C. Role of the Intravoxel Incoherent Motion Diffusion Weighted Imaging in the Pre-treatment Prediction and Early Response Monitoring to Neoadjuvant Chemotherapy in Locally Advanced Breast Cancer. *Medicine* (Baltimore) 2016; **95**: e2420 [PMID: 26825883 DOI: 10.1097/md.0000000000002420]
67 **Gaeta M**, Benedetto C, Minutoli F, D'Angelo T, Amato E, Mazziotti S, Racchiusa S, Mormina E, Blandino A, Pergolizzi S. Use of diffusion-weighted, intravoxel incoherent motion, and dynamic contrast-enhanced MR imaging in the assessment of response to radiotherapy of lytic bone metastases from breast cancer. *Acad Radiol* 2014; **21**: 1286-1293 [PMID: 25088834 DOI: 10.1016/j.acra.2014.05.021]
68 **Joo I**, Lee JM, Han JK, Choi BI. Intravoxel incoherent motion diffusion-weighted MR imaging for monitoring the therapeutic efficacy of the vascular disrupting agent CKD-516 in rabbit VX2 liver tumors. *Radiology* 2014; **272**: 417-426 [PMID: 24697148 DOI: 10.1148/radiol.14131165]
69 **Joo I**, Lee JM, Grimm R, Han JK, Choi BI. Monitoring Vascular Disrupting Therapy in a Rabbit Liver Tumor Model: Relationship between Tumor Perfusion Parameters at IVIM Diffusion-weighted MR Imaging and Those at Dynamic Contrast-enhanced MR Imaging. *Radiology* 2016; **278**: 104-113 [PMID: 26200601 DOI: 10.1148/radiol.2015141974]
70 **Koh DM**. Science to practice: can intravoxel incoherent motion diffusion-weighted MR imaging be used to assess tumor response to antivascular drugs? *Radiology* 2014; **272**: 307-308 [PMID: 25058129 DOI: 10.1148/radiol.14140714]
71 **Guo Z**, Zhang Q, Li X, Jing Z. Intravoxel Incoherent Motion Diffusion Weighted MR Imaging for Monitoring the Instantly Therapeutic Efficacy of Radiofrequency Ablation in Rabbit VX2 Tumors without Evident Links between Conventional Perfusion Weighted Images. *PLoS One* 2015; **10**: e0127964 [PMID: 26020785 DOI: 10.1371/journal.pone.0127964]
72 **Shirota N**, Saito K, Sugimoto K, Takara K, Moriyasu F, Tokuuye K. Intravoxel incoherent motion MRI as a biomarker of sorafenib treatment for advanced hepatocellular carcinoma: a pilot study. *Cancer Imaging* 2016; **16**: 1 [PMID: 26822946 DOI: 10.1186/s40644-016-0059-3]
73 **Granata V**, Fusco R, Catalano O, Filice S, Amato DM, Nasti G, Avallone A, Izzo F, Petrillo A. Early assessment of colorectal cancer patients with liver metastases treated with antiangiogenic drugs: The role of intravoxel incoherent motion in diffusion-weighted imaging. *PLoS One* 2015; **10**: e0142876 [PMID: 26566221 DOI: 10.1371/journal.pone.0142876]
74 **Park YS**, Lee CH, Kim JH, Kim IS, Kiefer B, Seo TS, Kim KA, Park CM. Using intravoxel incoherent motion (IVIM) MR imaging to predict lipiodol uptake in patients with hepatocellular carcinoma following transcatheter arterial chemoembolization: a preliminary result. *Magn Reson Imaging* 2014; **32**: 638-646 [PMID: 24703575 DOI: 10.1016/j.mri.2014.03.003]
75 **Hori M**, Fukunaga I, Masutani Y, Taoka T, Kamagata K, Suzuki Y, Aoki S. Visualizing non-Gaussian diffusion: clinical application of q-space imaging and diffusional kurtosis imaging of the brain and spine. *Magn Reson Med Sci* 2012; **11**: 221-233 [PMID: 23269009 DOI: 10.2463/mrms.11.221]
76 **Rosenkrantz AB**, Padhani AR, Chenevert TL, Koh DM, De Keyzer F, Taouli B, Le Bihan D. Body diffusion kurtosis imaging: Basic principles, applications, and considerations for clinical practice. *J Magn Reson Imaging* 2015; **42**: 1190-1202 [PMID: 26119267 DOI: 10.1002/jmri.24985]
77 **Sun PZ**, Wang Y, Mandeville E, Chan ST, Lo EH, Ji X. Validation of fast diffusion kurtosis MRI for imaging acute ischemia in a rodent model of stroke. *NMR Biomed* 2014; **27**: 1413-1418 [PMID: 25208309 DOI: 10.1002/nbm.3188]
78 **Zhao L**, Wang Y, Jia Y, Zhong S, Sun Y, Zhou Z, Zhang Z, Huang L. Cerebellar microstructural abnormalities in bipolar depression and unipolar depression: A diffusion kurtosis and perfusion imaging study. *J Affect Disord* 2016; **195**: 21-31 [PMID: 26852094 DOI: 10.1016/j.jad.2016.01.042]
79 **Kamiya K**, Kamagata K, Miyajima M, Nakajima M, Hori M, Tsuruta K, Mori H, Kunimatsu A, Arai H, Aoki S, Ohtomo K. Diffusional Kurtosis Imaging in Idiopathic Normal Pressure Hydrocephalus: Correlation with Severity of Cognitive Impairment. *Magn Reson Med Sci* 2016; Epub ahead of print [PMID: 26841854 DOI: 10.2463/mrms.mp.2015-0093]
80 **Yuan L**, Sun M, Chen Y, Long M, Zhao X, Yin J, Yan X, Ji D, Ni H. Non-Gaussian diffusion alterations on diffusion kurtosis imaging in patients with early Alzheimer's disease. *Neurosci Lett* 2016; **616**: 11-18 [PMID: 26797581 DOI: 10.1016/j.neulet.2016.01.021]
81 **Jiang R**, Jiang J, Zhao L, Zhang J, Zhang S, Yao Y, Yang S, Shi J, Shen N, Su C, Zhang J, Zhu W. Diffusion kurtosis imaging can efficiently assess the glioma grade and cellular proliferation. *Oncotarget* 2015; **6**: 42380-42393 [PMID: 26544514 DOI: 10.18632/oncotarget.5675]
82 **Tyagi N**, Riaz N, Hunt M, Wengler K, Hatzoglou V, Young R, Mechalakos J, Lee N. Weekly response assessment of involved lymph nodes to radiotherapy using diffusion-weighted MRI in oropharynx squamous cell carcinoma. *Med Phys* 2016; **43**: 137 [PMID: 26745906 DOI: 10.1118/1.4937791]
83 **Chen Y**, Ren W, Zheng D, Zhong J, Liu X, Yue Q, Liu M, Xiao Y, Chen W, Chan Q, Pan J. Diffusion kurtosis imaging predicts neoadjuvant chemotherapy responses within 4 days in advanced nasopharyngeal carcinoma patients. *J Magn Reson Imaging* 2015; **42**: 1354-1361 [PMID: 25873208 DOI: 10.1002/jmri.24910]
84 **Rosenkrantz AB**, Sigmund EE, Winnick A, Niver BE, Spieler B, Morgan GR, Hajdu CH. Assessment of hepatocellular carcinoma using apparent diffusion coefficient and diffusion kurtosis indices: preliminary experience in fresh liver explants. *Magn Reson Imaging* 2012; **30**: 1534-1540 [PMID: 22819175 DOI: 10.1016/j.mri.2012.04.020]
85 **Filli L**, Wurnig M, Nanz D, Luechinger R, Kenkel D, Boss A. Whole-body diffusion kurtosis imaging: initial experience on non-Gaussian diffusion in various organs. *Invest Radiol* 2014; **49**: 773-778 [PMID: 24979203 DOI: 10.1097/rli.0000000000000082]
86 **Goshima S**, Kanematsu M, Noda Y, Kondo H, Watanabe H, Bae KT. Diffusion kurtosis imaging to assess response to treatment in hypervascular hepatocellular carcinoma. *AJR Am J Roentgenol* 2015; **204**: W543-W549 [PMID: 25905960 DOI: 10.2214/ajr.14.13235]
87 **Martín Noguerol T**, Sánchez-González J, Martínez Barbero JP, García-Figueiras R, Baleato-González S, Luna A. Clinical Imaging of Tumor Metabolism with ^{1}H Magnetic Resonance Spectroscopy. *Magn Reson Imaging Clin N Am* 2016; **24**: 57-86 [PMID: 26613876 DOI: 10.1016/j.mric.2015.09.002]
88 **Kuo YT**, Li CW, Chen CY, Jao J, Wu DK, Liu GC. In vivo proton magnetic resonance spectroscopy of large focal hepatic lesions and metabolite change of hepatocellular carcinoma before and after transcatheter arterial chemoembolization using 3.0-T MR scanner. *J Magn Reson Imaging* 2004; **19**: 598-604 [PMID: 15112309 DOI: 10.1002/jmri.20046]
89 **Wu B**, Peng WJ, Wang PJ, Gu YJ, Li WT, Zhou LP, Tang F, Zhong GM. In vivo 1H magnetic resonance spectroscopy in evaluation of hepatocellular carcinoma and its early response to transcatheter arterial chemoembolization. *Chin Med Sci J* 2006; **21**: 258-264 [PMID: 17249202]
90 **Chen CY**, Li CW, Kuo YT, Jaw TS, Wu DK, Jao JC, Hsu JS, Liu GC. Early response of hepatocellular carcinoma to transcatheter

arterial chemoembolization: choline levels and MR diffusion constants--initial experience. *Radiology* 2006; **239**: 448-456 [PMID: 16569781 DOI: 10.1148/radiol.2392042202]

91 **Bonekamp S**, Shen J, Salibi N, Lai HC, Geschwind J, Kamel IR. Early response of hepatic malignancies to locoregional therapy-value of diffusion-weighted magnetic resonance imaging and proton magnetic resonance spectroscopy. *J Comput Assist Tomogr* 2011; **35**: 167-173 [PMID: 21412085 DOI: 10.1097/RCT.0b013e3182004bfb]

92 **Bian DJ**, Xiao EH, Hu DX, Chen XY, Situ WJ, Yuan SW, Sun JL, Yang LP. Magnetic resonance spectroscopy on hepatocellular carcinoma after transcatheter arterial chemoembolization. *Chin J Cancer* 2010; **29**: 198-201 [PMID: 20109351 DOI: 10.5732/cjc.009.10312]

93 **Sourbron S**. Technical aspects of MR perfusion. *Eur J Radiol* 2010; **76**: 304-313 [PMID: 20363574 DOI: 10.1016/j.ejrad.2010.02.017]

94 **Tofts PS**. Modeling tracer kinetics in dynamic Gd-DTPA MR imaging. *J Magn Reson Imaging* 1997; **7**: 91-101 [PMID: 9039598 DOI: 10.1002/jmri.1880070113]

95 **Huang B**, Wong CS, Whitcher B, Kwong DL, Lai V, Chan Q, Khong PL. Dynamic contrast-enhanced magnetic resonance imaging for characterising nasopharyngeal carcinoma: comparison of semiquantitative and quantitative parameters and correlation with tumour stage. *Eur Radiol* 2013; **23**: 1495-1502 [PMID: 23377545 DOI: 10.1007/s00330-012-2740-7]

96 **Xu H**, Xie JX, Li X, Yang ZH, Zheng ZZ, Wang B, Wang Z. Perfusion-weighted MRI in evaluating the intranodular hemodynamic characteristics of dysplastic nodules and hepatocellular carcinomas in an experimental rat model. *J Magn Reson Imaging* 2008; **27**: 102-109 [PMID: 18022847 DOI: 10.1002/jmri.21188]

97 **Chen X**, Xiao E, Shu D, Yang C, Liang B, He Z, Bian D. Evaluating the therapeutic effect of hepatocellular carcinoma treated with transcatheter arterial chemoembolization by magnetic resonance perfusion imaging. *Eur J Gastroenterol Hepatol* 2014; **26**: 109-113 [PMID: 24284371 DOI: 10.1097/MEG.0b013e328363716e]

98 **Chen BB**, Shih TT. DCE-MRI in hepatocellular carcinoma-clinical and therapeutic image biomarker. *World J Gastroenterol* 2014; **20**: 3125-3134 [PMID: 24695624 DOI: 10.3748/wjg.v20.i12.3125]

99 **Braren R**, Altomonte J, Settles M, Neff F, Esposito I, Ebert O, Schwaiger M, Rummeny E, Steingoetter A. Validation of preclinical multiparametric imaging for prediction of necrosis in hepatocellular carcinoma after embolization. *J Hepatol* 2011; **55**: 1034-1040 [PMID: 21354233 DOI: 10.1016/j.jhep.2011.01.049]

100 **Morgan B**, Utting JF, Higginson A, Thomas AL, Steward WP, Horsfield MA. A simple, reproducible method for monitoring the treatment of tumours using dynamic contrast-enhanced MR imaging. *Br J Cancer* 2006; **94**: 1420-1427 [PMID: 16670720 DOI: 10.1038/sj.bjc.6603140]

101 **Zhao JG**, Feng GS, Kong XQ, Li X, Li MH, Cheng YS. Assessment of hepatocellular carcinoma vascularity before and after transcatheter arterial chemoembolization by using first pass perfusion weighted MR imaging. *World J Gastroenterol* 2004; **10**: 1152-1156 [PMID: 15069716 DOI: 10.3748/wjg.v10.i8.1152]

102 **Zhao JG**, Feng GS, Kong XQ, Li X, Li MH, Cheng YS. Changes of tumor microcirculation after transcatheter arterial chemoembolization: first pass perfusion MR imaging and Chinese ink casting in a rabbit model. *World J Gastroenterol* 2004; **10**: 1415-1420 [PMID: 15133845 DOI: 10.3748/wjg.v10.i10.1415]

103 **Ogawa S**, Lee TM, Kay AR, Tank DW. Brain magnetic resonance imaging with contrast dependent on blood oxygenation. *Proc Natl Acad Sci USA* 1990; **87**: 9868-9872 [PMID: 2124706 DOI: 10.1073/pnas.87.24.9868]

104 **Pauling L**, Coryell CD. The Magnetic Properties and Structure of the Hemochromogens and Related Substances. *Proc Natl Acad Sci USA* 1936; **22**: 159-163 [PMID: 16588065 DOI: 10.1073/pnas.22.3.159]

105 **Wedegärtner U**, Popovych S, Yamamura J, Kooijman H, Adam G. DeltaR2* in fetal sheep brains during hypoxia: MR imaging at 3.0 T versus that at 1.5 T. *Radiology* 2009; **252**: 394-400 [PMID: 19546425 DOI: 10.1148/radiol.2522080844]

106 **Chalouhi GE**, Alison M, Deloison B, Thiam R, Autret G, Balvay D, Cuenod CA, Clément O, Salomon LJ, Siauve N. Fetoplacental oxygenation in an intrauterine growth restriction rat model by using blood oxygen level-dependent MR imaging at 4.7 T. *Radiology* 2013; **269**: 122-129 [PMID: 23696681 DOI: 10.1148/radiol.13121742]

107 **Nissen JC**, Mie MB, Zöllner FG, Haneder S, Schoenberg SO, Michaely HJ. Blood oxygenation level dependent (BOLD)--renal imaging: concepts and applications. *Z Med Phys* 2010; **20**: 88-100 [PMID: 20807689 DOI: 10.1016/j.zemedi.2010.01.003]

108 **Hofmann L**, Simon-Zoula S, Nowak A, Giger A, Vock P, Boesch C, Frey FJ, Vogt B. BOLD-MRI for the assessment of renal oxygenation in humans: acute effect of nephrotoxic xenobiotics. *Kidney Int* 2006; **70**: 144-150 [PMID: 16641929 DOI: 10.1038/sj.ki.5000418]

109 **Chopra S**, Foltz WD, Milosevic MF, Toi A, Bristow RG, Ménard C, Haider MA. Comparing oxygen-sensitive MRI (BOLD R2*) with oxygen electrode measurements: a pilot study in men with prostate cancer. *Int J Radiat Biol* 2009; **85**: 805-813 [PMID: 19728195 DOI: 10.1080/09553000903043059]

110 **Zhao D**, Pacheco-Torres J, Hallac RR, White D, Peschke P, Cerdán S, Mason RP. Dynamic oxygen challenge evaluated by NMR T1 and T2*--insights into tumor oxygenation. *NMR Biomed* 2015; **28**: 937-947 [PMID: 26058575 DOI: 10.1002/nbm.3325]

111 **Belfatto A**, White DA, Zhang Z, Zhang Z, Cerveri P, Baroni G, Mason RP. Mathematical modeling of tumor response to radiation: radio-sensitivity correlation with BOLD, TOLD, ΔR1 and ΔR2* investigated in large Dunning R3327-AT1 rat prostate tumors. *Conf Proc IEEE Eng Med Biol Soc* 2015; **2015**: 3266-3269 [PMID: 26736989 DOI: 10.1109/embc.2015.7319089]

112 **Hallac RR**, Zhou H, Pidikiti R, Song K, Stojadinovic S, Zhao D, Solberg T, Peschke P, Mason RP. Correlations of noninvasive BOLD and TOLD MRI with pO2 and relevance to tumor radiation response. *Magn Reson Med* 2014; **71**: 1863-1873 [PMID: 23813468 DOI: 10.1002/mrm.24846]

113 **Choi JW**, Kim H, Kim HC, Lee Y, Kwon J, Yoo RE, Cho HR, Choi SH, Chung JW. Blood oxygen level-dependent MRI for evaluation of early response of liver tumors to chemoembolization: an animal study. *Anticancer Res* 2013; **33**: 1887-1892 [PMID: 23645735]

114 **Zhang LJ**, Zhang Z, Xu J, Jin N, Luo S, Larson AC, Lu GM. Carbogen gas-challenge blood oxygen level-dependent magnetic resonance imaging in hepatocellular carcinoma: Initial results. *Oncol Lett* 2015; **10**: 2009-2014 [PMID: 26622788 DOI: 10.3892/ol.2015.3526]

115 **Kim HO**, Kim JS, Shin YM, Ryu JS, Lee YS, Lee SG. Evaluation of metabolic characteristics and viability of lipiodolized hepatocellular carcinomas using 18F-FDG PET/CT. *J Nucl Med* 2010; **51**: 1849-1856 [PMID: 21098794 DOI: 10.2967/jnumed.110.079244]

116 **Mocherla B**, Kim J, Roayaie S, Kim S, Machac J, Kostakoglu L. FDG PET/CT imaging to rule out extrahepatic metastases before liver transplantation. *Clin Nucl Med* 2007; **32**: 947-948 [PMID: 18030049 DOI: 10.1097/RLU.0b013e3181598cef]

117 **Kim SH**, Won KS, Choi BW, Jo I, Zeon SK, Chung WJ, Kwon JH. Usefulness of F-18 FDG PET/CT in the Evaluation of Early Treatment Response After Interventional Therapy for Hepatocellular Carcinoma. *Nucl Med Mol Imaging* 2012; **46**: 102-110 [PMID: 24900042 DOI: 10.1007/s13139-012-0138-8]

118 **Zhao M**, Wu PH, Zeng YX, Zhang FJ, Huang JH, Fan WJ, Gu YK, Zhang L, Tan ZB, Lin YE. [Evaluating efficacy of transcatheter arterial chemo-embolization combined with radiofrequency ablation on patients with hepatocellular carcinoma by 18FDG-PET/CT]. *Ai Zheng* 2005; **24**: 1118-1123 [PMID: 16159437]

119 **Han AR**, Gwak GY, Choi MS, Lee JH, Koh KC, Paik SW, Yoo BC. The clinical value of 18F-FDG PET/CT for investigating unexplained serum AFP elevation following interventional therapy for hepatocellular carcinom. *Hepatogastroenterology* 2009; **56**: 1111-1116 [PMID: 19760952]

120 **Chen YK**, Hsieh DS, Liao CS, Bai CH, Su CT, Shen YY, Hsieh JF, Liao AC, Kao CH. Utility of FDG-PET for investigating unexplained serum AFP elevation in patients with suspected hepatocellular carcinoma recurrence. *Anticancer Res* 2005; **25**: 4719-4725 [PMID:

16334166]
121 **Boss A**, Bisdas S, Kolb A, Hofmann M, Ernemann U, Claussen CD, Pfannenberg C, Pichler BJ, Reimold M, Stegger L. Hybrid PET/MRI of intracranial masses: initial experiences and comparison to PET/CT. *J Nucl Med* 2010; **51**: 1198-1205 [PMID: 20660388 DOI: 10.2967/jnumed.110.074773]
122 **Boss A**, Kolb A, Hofmann M, Bisdas S, Nägele T, Ernemann U, Stegger L, Rossi C, Schlemmer HP, Pfannenberg C, Reimold M, Claussen CD, Pichler BJ, Klose U. Diffusion tensor imaging in a human PET/MR hybrid system. *Invest Radiol* 2010; **45**: 270-274 [PMID: 20351651 DOI: 10.1097/RLI.0b013e3181dc3671]
123 **Torigian DA**, Zaidi H, Kwee TC, Saboury B, Udupa JK, Cho ZH, Alavi A. PET/MR imaging: technical aspects and potential clinical applications. *Radiology* 2013; **267**: 26-44 [PMID: 23525716 DOI: 10.1148/radiol.13121038]
124 **Lee G**, I H, Kim SJ, Jeong YJ, Kim IJ, Pak K, Park do Y, Kim GH. Clinical implication of PET/MR imaging in preoperative esophageal cancer staging: comparison with PET/CT, endoscopic ultrasonography, and CT. *J Nucl Med* 2014; **55**: 1242-1247 [PMID: 24868109 DOI: 10.2967/jnumed.114.138974]
125 **Buchbender C**, Heusner TA, Lauenstein TC, Bockisch A, Antoch G. Oncologic PET/MRI, part 1: tumors of the brain, head and neck, chest, abdomen, and pelvis. *J Nucl Med* 2012; **53**: 928-938 [PMID: 22582048 DOI: 10.2967/jnumed.112.105338]
126 **Yu JS**, Chung JJ, Kim JH, Cho ES, Kim DJ, Ahn JH, Kim KW. Detection of small intrahepatic metastases of hepatocellular carcinomas using diffusion-weighted imaging: comparison with conventional dynamic MRI. *Magn Reson Imaging* 2011; **29**: 985-992 [PMID: 21616624 DOI: 10.1016/j.mri.2011.04.010]
127 **Tsouana E**, Stoneham S, Fersht N, Kitchen N, Gaze M, Bomanji J, Fraioli F, Hargrave D, Shankar A. Evaluation of treatment response using integrated 18F-labeled choline positron emission tomography/magnetic resonance imaging in adolescents with intracranial non-germinomatous germ cell tumours. *Pediatr Blood Cancer* 2015; **62**: 1661-1663 [PMID: 25854508 DOI: 10.1002/pbc.25538]
128 **Fowler KJ**, Maughan NM, Laforest R, Saad NE, Sharma A, Olsen J, Speirs CK, Parikh PJ. PET/MRI of Hepatic 90Y Microsphere Deposition Determines Individual Tumor Response. *Cardiovasc Intervent Radiol* 2015; Epub ahead of print [PMID: 26721589 DOI: 10.1007/s00270-015-1285-y]
129 **Lipnick S**, Liu X, Sayre J, Bassett LW, Debruhl N, Thomas MA. Combined DCE-MRI and single-voxel 2D MRS for differentiation between benign and malignant breast lesions. *NMR Biomed* 2010; **23**: 922-930 [PMID: 20878970 DOI: 10.1002/nbm.1511]
130 **Faeghi F**, Baniasadipour B, Jalalshokouhi J. Comparative Investigation of Single Voxel Magnetic Resonance Spectroscopy and Dynamic Contrast Enhancement MR Imaging in Differentiation of Benign and Malignant Breast Lesions in a Sample of Iranian Women. *Asian Pac J Cancer Prev* 2015; **16**: 8335-8338 [PMID: 26745081]

P- Reviewer: Ooi LLPJ, Ramia JM **S- Editor**: Ma YJ
L- Editor: Wang TQ **E- Editor**: Wang CH

Published by **Baishideng Publishing Group Inc**
8226 Regency Drive, Pleasanton, CA 94588, USA
Telephone: +1-925-223-8242
Fax: +1-925-223-8243
E-mail: bpgoffice@wjgnet.com
Help Desk: http://www.wjgnet.com/esps/helpdesk.aspx
http://www.wjgnet.com

ISSN 1007-9327